Journal of Applied Polymer Science

Characterization of nanoclay intercalation during foaming with *in situ* energy-dispersive X-ray diffraction

J. Escudero,[1] B. Notario,[1] C. Jimenez,[2] M. A. Rodriguez-Perez[1]
[1]Cellular Materials Laboratory, Condensed Matter Physics Department, University of Valladolid, Valladolid, Spain
[2]Helmhotz-Zentrum Berlin, Hahn Meitner Platz 1, 14109, Berlin, Germany
Correspondence to: B. Notario (E-mail: belen.notario@fmc.uva.es)

ABSTRACT: The effect of the foaming process on the intercalation of nanoclays in low-density polyethylene–nanoclay nanocomposites was studied with *in situ* energy-dispersive X-ray diffraction (ED-XRD) with synchrotron radiation as an X-ray source. The solid nanocomposites containing different amounts of an organomodified montmorillonite were melt-blended with blowing agents of different nature and later foamed by heating at atmospheric pressure. During the foaming process, ED-XRD experiments were performed. These experiments allowed us to measure the time evolution of the interlamellar distance of the clay platelets during the melting and foaming of the nanocomposites; we obtained information about the evolution of the clay structure during the process. The experimental results show that the foaming process induced the intercalation of the clays independently of the blowing agent used. We also proved that the degree of intercalation depended on the expansion ratio reached and that the intercalation produced was larger when the blowing agent was azodicarbonamide. For this particular blowing agent, some interesting effects appeared; these included a catalytic effect of the clays on the decomposition temperature, a partial intercalation of the clays during melt blending, and a very stable structure of the clay particles after foaming. © 2016 Wiley Periodicals, Inc. J. Appl. Polym. Sci. **2016**, *133*, 43432.

KEYWORDS: clay; foams; properties and characterization; thermoplastics; X-ray

Received 9 November 2015; accepted 9 January 2016
DOI: 10.1002/app.43432

INTRODUCTION

During the last decade, the excellent properties of clay–polymer nanocomposites (CPNC) have stimulated much interest and research within the scientific and industrial communities. The high surface-to-volume ratio of nanoclays leads to a high reinforcement efficiency. Thus, clay–polymer nanocomposites with well-dispersed and exfoliated platelets at a low clay loading show increased modulus and yield strength and reduced flame propagation and permeability.[1,2] In addition, in semicrystalline polymers, clay platelets can promote faster crystallization and higher levels of crystallinity; this results in improved solvent and moisture resistance but reduced impact strength.[1,3–5]

There are three basic structures for polymer–clay mixtures: conventional clay-filled composites with micrometer-sized aggregates of clay particles, nanocomposites with intercalated clay with a locally ordered structure, and exfoliated nanocomposites with a disordered structure. Not all performance characteristics depend to the same degree on exfoliation; however, the benefits increase with the degree of intercalation–exfoliation of the clay platelets. Thus, the goal of clay–polymer nanocomposite technology is to achieve the highest possible degree of clay intercalation–exfoliation. Currently, three main methods for achieving it can be distinguished[3,5]:

1. Polymerization in the presence of organoclay.
2. Melt compounding a polymer with a suitable organoclay complex.
3. Other methods, such as ultrasonic exfoliation of organoclays in a low-molecular-weight polar liquid or coprecipitation.[6–8]

Numerous examples of nanocomposites based on very different polymers and produced by any of the three previously mentioned routes can be found in the literature.[9–12] This work and the corresponding revision of the state of the art is focused on nanocomposites produced from polyethylene (PE). The nonpolar character of PE makes it difficult to obtain an exfoliated structure. The first two methods are the most examined ones. Polymerization in the presence of organoclays fundamentally consists of the intercalation of the clay with a compound that subsequently enters the polymerization reaction (either polycondensation or radical polymerization). Jin *et al.*[13] reported the full exfoliation of a PE–montmorillonite (MMT) system prepared by the Ziegler–Natta polymerization of ethylene in the presence of organoclay. Although after polymerization the

degree of exfoliation was high, a partial reaggregation of MMT platelets occurred after processing by compression molding. Alexandre *et al.*[14] polymerized PE in the presence of either MMT or hectorite. Clay exfoliation in the reaction products was confirmed by X-ray diffraction and transmission electron microscopy, but the tensile properties of the resulting nanocomposites were poor and essentially independent of the nature and content of the silicate. Moreover, during melt processing, the interlayer spacing partially collapsed.

Melt blending is the preferred method for preparing clay–polymer nanocomposites with thermoplastic polymer matrices. Typically, the polymer is melted and combined with the desired amount of clay in an extruder or internal mixer. Wang *et al.*[15] produced PE–clay nanocomposites by melt blending and determined their flammable properties. The heat-release rate was reduced by 32% for the nanocomposites in comparison to the raw PE. The microstructure and mechanical properties of PE–clay melt-blended nanocomposites were determined by Liang *et al.*[16] To improve the nanoclay exfoliation, a coupling agent based on maleic anhydride grafted PE was used. Important improvements were found in the tensile and impact strengths at a clay loading of 6 wt %. Thermodynamically, the melt-blended nanocomposites were stable, but the achievement of fully exfoliated morphologies was not easy. Commonly, nanocomposites exhibit more attainable intercalated–exfoliated structures with higher or lower degrees of exfoliation, depending on the specific system and preparation method used.

Cellular nanocomposites are currently subject to attention in both the scientific and industrial communities. The combination of functional nanoparticles and foaming technologies has a high potential to generate materials that are lightweight and multifunctional and have a high stiffness and strength-to-weight ratio.[17] As a result of these expected outstanding properties, the number of works dealing with the production and characterization of cellular nanocomposites has rapidly increased in the last few years. Efforts have been focused both on thermoplastic (amorphous and semicrystalline) and thermoset polymers. The infused nanoparticles have been also very diverse, from carbon nanotubes to carbon nanofibers or silica particles. In addition, nanoclays have also been used in a very important number of the works already published.[18–27] Most of these works are related to the observed properties of the cellular material (thermal, mechanical, fire-resistance, and gas-barrier properties) and the state of aggregation and dispersion of the nanoparticles in the solid matrix before foaming. However, in general, the analysis of the possible evolution of the intercalation–exfoliation degree of clay particles during the foaming process has not been analyzed in detail.

An interesting result was found by Velasco and coworkers[28,29] a few years ago. They showed that the degree of exfoliation was enhanced after the foaming process. The cellular polymers were produced from a melt-blended nanocomposite based on PE and hectorite. The solid matrix before foaming presented an intercalated–exfoliated structure. The state of delamination of the nanoclays was characterized by the determination of the X-ray diffraction pattern before and after foaming and their comparison. They showed that the produced foams presented a higher degree of intercalation–exfoliation than the initial solid precursors; thus, it seemed that the foaming processes induced a modification of the clay structure.

The *ex situ* study of the samples reported in that article showed interesting results about intercalation–exfoliation but did not provide insights into the mechanisms involved. Among others, the following aspects are still unknown:

- The previous observed effects were obtained with azodicarbonamide (AZO) as the blowing agent, but there are not results about other blowing agents.
- It is not known whether foaming is the only factor that produces the increment in interlamellar spacing or other thermal processes, such as whether polymer melting has also an effect.
- It is not clear if the intercalation–exfoliation degree observed after foaming and the solidification of the foam is the maximum reached or there is a higher value during intermediates state.
- It is unknown whether foam collapse and solidification have an effect on the intercalation–exfoliation degree.
- There is a lack of knowledge about the influence of the blowing agent content and hence of the expansion ratio achieved on the interlamellar spacing.
- The amount of nanoclays could also play some role that has not been described so far.

To answer all of these questions and gain knowledge on the mechanisms underlying this interesting effect, we performed an *in situ* study with synchrotron radiation. In this way, the whole behavior was characterized, from the diffraction pattern of the solid precursor passing through all of the intermediate states up to the final solidified foam.

With the previous ideas in mind, in this work, we used an energy-dispersive X-ray diffraction (ED-XRD) technique with a synchrotron light source to follow *in situ* the evolution of the interlamellar spacing during foaming in the PE–MMT systems. The *in situ* technique was combined with blowing agents of different nature, different contents of the same blowing agent, and different additions of nanoclays to gain knowledge about the mechanisms underlying the modification of the clay structure during foaming.

EXPERIMENTAL

The intercalation of nanoclays during foaming was followed *in situ* by ED-XRD at the EDDi experimental station hosted at the BESSY II synchrotron light source of the Helmholtz Centre Berlin (Figure 1). Samples were illuminated by a white X-ray beam with a $2 \times 1\,mm^2$ (Height $\times$ Width) cross section. The peaks of intensity were detected at particular energies (E_{hkl}'s) in transmission geometry at an angle of $2\theta = 1.7°$ by a Ge multichannel analyzing detector because the diffracted photon energies obeyed Bragg's law, which reads in its energy-dispersive form as follows:

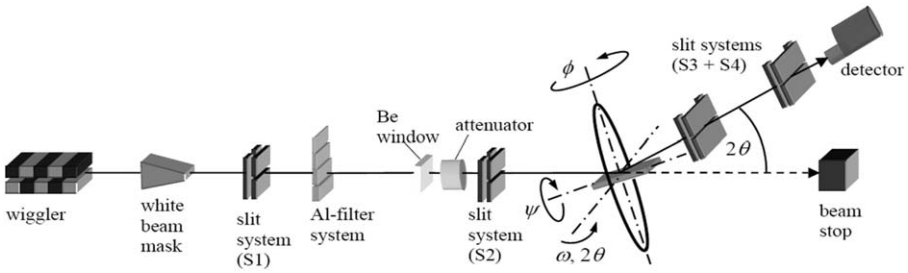

Figure 1. EDDi experimental station hosted at the BESSY II synchrotron light source. The beam crosses a system of slits, filters, and attenuators before hitting the sample.

$$E_{hkl}=hc/2d_{hkl}\theta$$

where h is Planck's constant, c is the speed of light, d_{hkl} is the interlamellar distance and θ is the angle between the incident rays and the planes of dispersion.

A self-designed X-ray transparent furnace equipped with IR lamps and Kapton windows was mounted on a positioning table attached to a goniometer. The sample size was $20 \times 10 \times 4\,mm^3$. The 10-mm side was placed parallel to the beam direction, and the 4-mm side indicated the compaction direction during the production of the precursor material. A thermocouple was inserted into the sample parallel to the 20-mm side and beside the beam path for recording and controlling the temperature with a CAL3300 controller and a self-developed program that ran under LabView. The temperature was increased from 30 °C up to the foaming temperatures (185 or 190 °C) at 10 K/min and held there for an isothermal step. After 600 s, the IR lamps were turned off, and cooling took place. The ED-XRD data acquisition and positioning table were computer-controlled by the software package Spec. Acquisition started when the sample temperature was 100 °C on heating. The counting time per spectrum was 30 s, after which a lateral sample displacement of 1 mm was programed to detect each time-diffracted photon energy from a volume that was previously not irradiated by the X-rays. Complementary spectra were also acquired for 30 s at room temperature, before heating and after cooling.

The following procedure was used to follow the increment of the interlamellar spacing during foaming. For each spectrum, the energy corresponding to the maximum of the nanoclay peak was calculated and converted into distance according to the following formula:

$$d_{hkl}=hc/2E_{hkl}\sin\theta$$

The obtained distance was plotted as a function of the foaming time. Because the acquisition of each spectrum lasted 30 s, the midpoint of the 30 s was selected as representative.

The density of the final foams produced in the *in situ* experiments was measured with Archimedes principle in a density-determination kit designed for the AT261 Mettler balance. In addition, for some of the formulations, on the basis of AZO as the blowing agent, thermogravimetric analysis experiments were carried out to evaluate the kinetics of gas release. The instrument used for thermogravimetric analysis was a TGA/SDTA 861 instrument from Mettler with a temperature program similar to the one used in the *in situ* experiments.

Materials

Low-density polyethylene (LDPE; PE003 from Repsol Alcudia), with a melt flow index of 2 g/10 min (measured at 190 °C and 2.16 kg), a density of 920 kg/m^3, and a melting temperature of 110 °C, was used as the polymer matrix. For the nanocomposites, this polymer matrix was melt-blended with the MMT-type organomodified nanoclay Cloisite C15A from Southern Clay Products and a coupling agent, maleic anhydride grafted PE Fusabond 226 DE from DuPont (melt flow index = 1.5 g/10 min at 190 °C and melting temperature = 120 °C). The blending was performed in a twin-screw extruder Bühler BTSK 20/40D at 250 rpm with a die temperature of 190 °C. The proportion of coupling agent to nanoclays was maintained constant at 2:1.

To study the foaming behavior, the previous nanocomposites were blended with three different blowing agents [4, 7, and 10 wt % AZO, 3 wt % Hydrocerol (HY), and 4 wt % Expancel (EXP)] and antioxidants Irgafos 168 (from Ciba) in a proportion of 0.08 wt % and Irganox 1010 (from Ciba) in a proportion of 0.02 wt % to prevent thermal oxidation of the polymer. The amounts of the different blowing agents were selected according to previous experiences. The blending of the nanocomposite with the blowing agents was performed in a twin-screw extruder (Collin mod ZK25T) ratio between the length and the diameter of the extruder (L/D). To prevent any difference in the intercalation–exfoliation of the platelets during blending, a constant-shear mixing energy was used for all of the samples. A screw speed of 50 rpm was used in all of the formulations with a constant feeding speed and a temperature profile identical for all of the compositions. This was varied from 105 °C in the hopper to 125 °C in the die in steps of 5 °C. Such a profile was chosen to prevent premature decomposition of the blowing agents during the compounding steps. The materials were water-cooled and pelletized.

The three specific blowing agents that were used were

- AZO (Porofor ADC/M-C1 from Lanxess): an exothermic chemical foaming agent presented as a yellow powder with an average particle size of $3.9 \pm 0.6\,\mu m$ and an onset of decomposition around 210 °C. The main released gases are N_2 (62%), CO (35%), and NH_3 (ca. 3%).[30,31]
- HY (BIH 40 E from Clariant): an endothermic chemical foaming agent masterbatch (in the form of white pellets with 60% active compound and an onset of decomposition of 140 °C). These blowing agents are mainly compounds of

Table I. Proportions of Components for the Different Kinds of Samples and the Foaming Temperatures

Sample	Matrix (parts)	Coupling agent (parts)	Nanoclays (parts)	Blowing agent (wt %)	Foaming temperature (°C)
5% Nanoclays_AZO4_185	85	10	5	4	185
5% Nanoclays_AZO4_190	85	10	5	4	190
3% Nanoclays_AZO7_185	91	6	3	7	185
3% Nanoclays_AZO7_190	91	6	3	7	190
5% Nanoclays_AZO7_185	85	10	5	7	185
5% Nanoclays_AZO7_190	85	10	5	7	190
5% Nanoclays_AZO10_185	85	10	5	10	185
5% Nanoclays_AZO10_190	85	10	5	10	190
5% Nanoclays_HY_185	85	10	5	3	185
5% Nanoclays_HY_190	85	10	5	3	190
5% Nanoclays_EXP_185	85	10	5	4	185
5% Nanoclays_EXP_190	85	10	5	4	190

alkali carbonate, citric acid, and citric acid esters in a carrier based in LDPE. The main products released in the decomposition are CO_2 and H_2O.[32–34]

- EXP (950 DU 80 from AkzoNobel): microspheres with a particle size between 18 and 24 μm and a density of 12 kg/m^3 or lower (once expanded) and are characterized by having a gas, typically a hydrocarbon, inside of them. The onset of activation is around 140 °C. Unlike the others, with the two blowing agents mentioned previously, once the temperature of decomposition is reached, a gas phase is released; in this case, when the activation temperature is reached, the microspheres start to expand and maintain most of the gas confined within.[35,36]

Before the foaming experiments, the formulations containing the different blowing agents were compression-molded into precursors with dimensions of 20 x 10 mm^2 and a thickness of 4 mm with a two-hot-plate press. In all of the formulations, the temperature of the press was fixed at 125 °C (lower than the decomposition point of all of the used blowing agents). The material was first melted without pressure for 15 min; then, it was pressed under a constant pressure of 2.18 MPa for another 15 min, and finally, it was cooled down under the same pressure. These molded precursors were used for the foaming tests.

For the samples containing AZO, three different contents were studied, 4, 7, and 10 wt %. In addition, two different clay contents were used for the materials containing 7% AZO. Two different foaming temperatures, 185 and 190 °C, were also used for all of the samples. The nominal compositions and nomenclature used for all of the analyzed materials are summarized in Table I.

RESULTS AND DISCUSSION

The effects of different variables were analyzed. In particular, the effects of the nature and content of the blowing agent and the content of the nanoparticles were studied.

Effects Related to the Nature of the Blowing Agent

The 5 wt % nanoclay filled samples were foamed with the three blowing agents at two different foaming temperatures (185 and 190 °C).

The interlamellar spacing obtained from the *in situ* diffractograms is presented in Figure 2 as a function of the foaming time for the two foaming temperatures. The sample temperature profile is also included in the figure. The trends observed were very similar for the two temperatures tested. The point corresponding to time 0 s corresponded to the *in situ* diffractogram of the solid precursor (i.e., the solid precursor material before foaming). The point corresponding to time 4500 s corresponded to the *in situ* diffractogram of the solidified foam (i.e., the final foam at room temperature).

Initially, at a time of 0 s, the separation between platelets in the samples blended with AZO was 10% higher than the one in samples blended with HY or EX. Therefore, AZO helped to increase the interlamellar spacing of the clays during melt blending; this indicated some type of chemical interaction between them.

The thermally activated higher mobility of the polymer molecular chains and the thermal expansion of the polymer helped to separate the nanoclay platelets at temperatures below the activation temperature of the blowing agents. This was observed from the interlamellar spacing value found at a time of about 200 s; this corresponded to a temperature of 110 °C. This value was 5% higher than that of the initial platelet separation. This increment, attributed to the thermal movement of the polymer chains and the thermal expansion of the polymeric matrix, was found independently of the blowing agent used and, for all of them, had a value near 5%.

In the samples containing AZO, from around 400 s, the rate of increment in the interlamellar spacing was higher. At that time, the sample temperature reached the decomposition temperature of the AZO. The foaming began and, hence, the interlamellar spacing increased at a higher rate than it did previously. This effect was not observed with HY or EX because the decomposition temperature windows of these two blowing agents were broader.[32–36] In any case, during the foaming process with these two blowing agents, there was also an increase in the intercalation of the clays. In the case of EX, the gas was mainly confined inside the microspheres at every

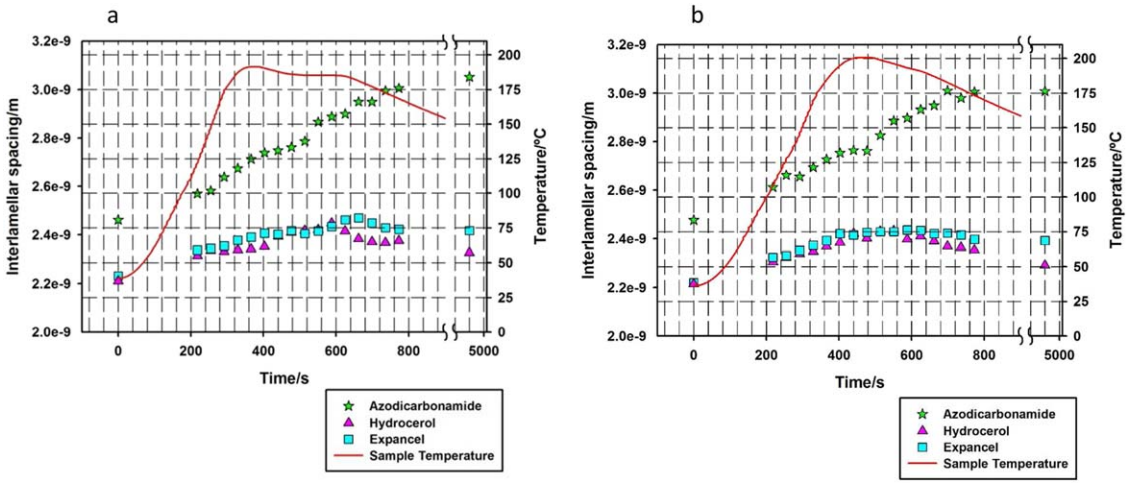

Figure 2. Evolution during foaming of the interlamellar spacing of the clay platelets at foaming temperatures of (a) 185 and (b) 190 °C. [Color figure can be viewed in the online issue, which is available at wileyonlinelibrary.com.]

moment; therefore, the increment in the intercalation was attributed to a separation because of the stretching of the polymer chains chemically bonded to the nanoclay platelets. In the case or HY, the main gas released was CO_2, which promoted a very similar expansion ratio (density of the solid matrix divided by the density of final foam) and similar intercalation to those of EX.

The final expansion ratios reached in each sample are shown in Table II. The expansion ratios achievable with AZO were higher than the ones achievable with HY or EX. This was probably one of the main reasons behind the lower increments in interlamellar spacing found for the samples containing HY or EX in comparison with the AZO ones (see later). Moreover, for the HY and EXP, the interlamellar spacing reached a maximum and then decayed to a lower value as the foam collapsed and/or solidified. On the contrary, with AZO, the volume reduction at the end of the experiment due to collapse and solidification (foam collapse and solidification were confirmed with optical *ex situ* optical expandometry) of the foam did not have any influence on the interlamellar spacing; the value reached during foaming was maintained level even when the foam was solidified. Therefore, it seemed that the chemical interaction between clay platelets and AZO proposed previously could also help to retain the maximum separation achieved between the platelets. The platelets were hooked to their new positions. Because HY and EX did not show any interaction with the layered silicates, the foam collapsed, and solidification also produced some collapse on the lamellar structure. On the other hand, the effect of the temperature on the final density is also shown in Table II. For two of the blowing agents, HY and EX, the effect of the temperature was not appreciable; this was probably because the activation temperature of the two blowing agents was well below the foaming temperature used in this study. For the material foamed with AZO, there was a decrease in the density when the foaming temperature increased; this should have been due to the higher amount of gas released when the foaming experiment was carried out at higher temperatures.

Effects Related to the Amount of the Blowing Agent

Three different amounts of the blowing agent that presented the most interesting results (AZO) were used for this study. Two different temperatures were also used, 185 and 190 °C.

The results are shown in Figure 3. The first remarkable result was found in the initial degree of intercalation at a time of 0 s. The higher the addition of blowing agent was, the higher the initial separation between platelets was. This result supported the hypothesized AZO–nanoclay chemical interaction, and because of this, an increase in the amount of blowing agent promoted a higher value for the interlamellar distance.

The same trend observed previously (Figure 2) was also observed in the results of Figure 3. At low temperatures (below the decomposition temperature of the blowing agent), there was an increase in the interlamellar spacing because of the mobility and thermal expansion of the polymer. This increment was found independently of the amount of blowing agent used and, for all of them, showed a value near 5%.

The interlamellar spacing continued increasing when the gas was released. At both temperatures, the highest expansion ratios (lower densities) were achieved with the samples containing 7 wt % AZO, as shown in Table III. This was translated again to

Table II. Final Densities and Expansion Ratios Achieved with the Different Blowing Agents at 185 and 190 °C

Sample	Density (kg/m^3)	Expansion ratio
5% Nanoclays_AZO7_185	250.3	3.7
5% Nanoclays_HY_185	648.0	1.3
5% Nanoclays_EXP_185	609.5	1.6
5% Nanoclays_AZO7_190	237.8	3.9
5% Nanoclays_HY_190	639.8	1.4
5% Nanoclays_EXP_190	616.8	1.5

The maximum expansion ratios achievable with EX and HY were lower than those obtained with AZO.

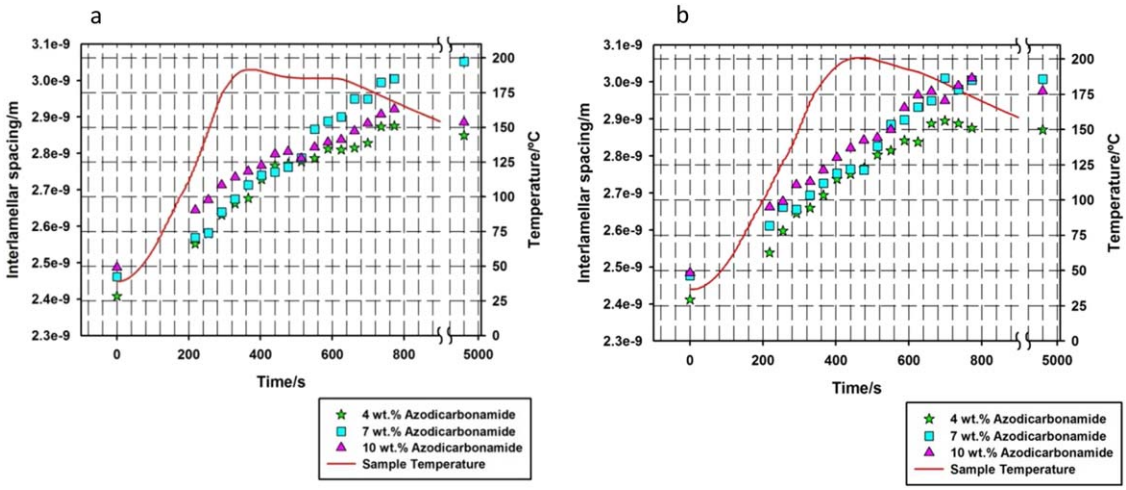

Figure 3. Evolution during foaming of the separation between platelets for materials containing different amounts of AZO at foaming temperatures of (a) 185 and (b) 190 °C. [Color figure can be viewed in the online issue, which is available at wileyonlinelibrary.com.]

the highest increments in interlamellar spacing (Figure 3) that were clearly reached for the materials containing 7% AZO. On the other hand, the amount of gas that was released in the 5% Nanoclays_AZO4 sample was lower, and hence, foaming ended earlier. Therefore, the maximum value of interlamellar spacing was reached at lower times than in the samples containing 7 and 10 wt % AZO. For the three analyzed compositions, the maximum degree of exfoliation reached was almost maintained after the solidification of the foam; this confirmed the effect mentioned in the previous section for this type of blowing agent.

As shown in Table III, the minimum density was reached for an intermediate content of AZO; the reason behind this behavior could have been related to the fact that an increasing amount of gas was not always connected to a density reduction because, when the amount of gas was very high, the polymer was not be able to tolerate the high stretching forces promoted by the pressure created by the blowing agent, and strong coalescence took place.[37] In general, the density reached was slightly reduced when the temperature was increased; this was due to the higher amount of gas generated at higher temperatures.

Effects Related to the Amount of the Nanoclays

As already mentioned, two different contents of nanoclays were studied, with the kind (AZO) and amount of blowing agent (7 wt %) fixed. Table IV shows the final densities achieved for the different samples. A large addition of nanoclays yielded also higher expansion ratios. There were several reasons behind this result. The first reason was related to a catalytic effect of the nanoclays over the AZO; this finally yielded a higher amount of gas released. This catalytic effect was analyzed with thermogravimetry, as shown in Figure 4. Blank for 3% and Blank for 5% are samples without nanoclays but with the same coupling agent–polymer matrix ratio maintained and the same amount of blowing agents as in the samples with clays. The weight loss measured by thermogravimetry was due to the decomposition of the AZO and, therefore, to the gas released. As inferred from Figure 4, the higher the addition of clays was, the higher the amount of gas was released at a given temperature, and therefore, higher expansion ratios were achieved. Not only was the

Table III. Final Densities and Expansion Ratios for Samples with Different AZO Additions

Sample	Density (kg/m^3)	Expansion ratio
5% Nanoclays_AZO4_185	293.7	3.2
5% Nanoclays_AZO7_185	250.3	3.7
5% Nanoclays_AZO10_185	287.7	3.2
5% Nanoclays_AZO4_190	294.9	3.1
5% Nanoclays_AZO7_190	237.8	3.9
5% Nanoclays_AZO10_190	261.3	3.6

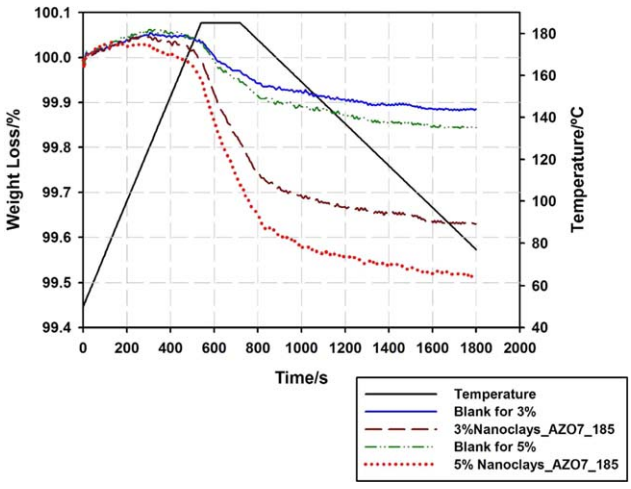

Figure 4. Weight loss measured by thermogravimetry due to the decomposition of AZO in samples containing different amounts of nanoclays and corresponding blank samples. The experiments were performed with a temperature program similar to the one used in the diffraction tests. [Color figure can be viewed in the online issue, which is available at wileyonlinelibrary.com.]

Table IV. Final Densities and Corresponding Expansion Ratios Achieved in Samples with Different Contents of Nanoclays

Sample	Density (kg/m^3)	Expansion ratio
3% Nanoclays_AZO7_185	324.2	2.8
5% Nanoclays_AZO7_185	250.3	3.7
3% Nanoclays_AZO7_190	313.1	2.9
5% Nanoclays_AZO7_190	237.8	3.9

amount of gas released higher in the samples with clays, but also the decomposition began earlier in these samples (Figure 4). In addition, the nanoclays might have also helped to increase the stability of the polymer melt during the foaming. This allowed the retention of more gas and finally translated into lower densities. Finally, the presence of nanoclays could have also played a gas-barrier role, limiting the gas escape and increasing the amount of gas available during foam expansion.

Figure 5 shows the evolution of interlamellar spacing for the samples containing different amounts of clay particles. The trends were similar to those shown in previous figures. It was clear that the samples containing 5 wt % showed a higher increase in the interlamellar distance; this was related to the higher expansion ratio reached in these materials.

The increment in interlamellar spacing attributed to the thermally activated mobility of the molecular chains was again observed independently of the nanoclay addition for temperatures below the decomposition temperature of the blowing agent. For higher temperatures, the material containing a higher amount of clays produced a higher separation of the clay platelets.

Correlation of the Expansion Ratio and the Increment in Interlamellar Spacing

Almost all of the samples studied fit well to a linear regression between the final expansion ratio and the increment (in percentage) in the interlamellar spacing, as shown in Figure 6. Independently of the kind of blowing agent used or gas released during the foaming, there was an increase in the interlamellar spacing associated with foaming. The higher the expansion ratio was reached, the higher the intercalation of the nanoclays was. This increment in the separation between platelets was as high as 24% for samples expanding more than 3.5 times.

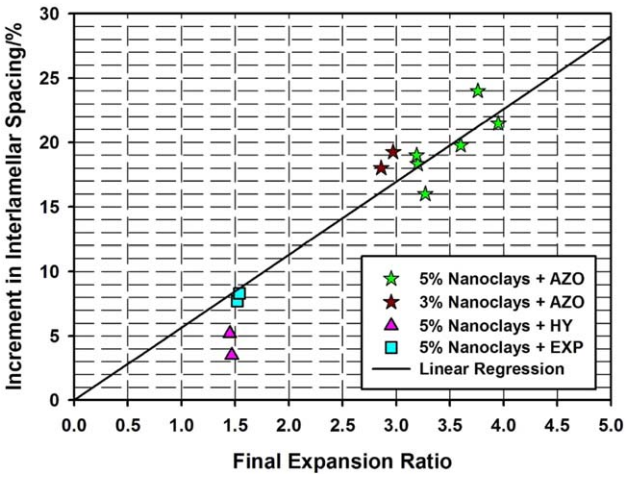

Figure 6. Correlation between the expansion ratio and the increment in interlamellar spacing (as a percentage) for the different blowing agents and different materials. [Color figure can be viewed in the online issue, which is available at wileyonlinelibrary.com.]

Samples containing HY (triangles in Figure 6) were below the linear regression. As it was previously studied, in these samples, the lamellar structure of the nanoclays presented a strong collapse matching with the collapse and solidification of the foam. Although the samples containing EX also presented some collapse after the maximum separation between platelets was reached; this collapse was not so strong. On the other hand, samples containing AZO maintained the maximum separation between platelets, even during the collapse of the foam cellular structure and solidification of the polymer. That was the reason why almost all of the samples containing AZO were near or above the linear regression. The fundamental reason explaining these differences is still unknown, and further research on this topic is needed.

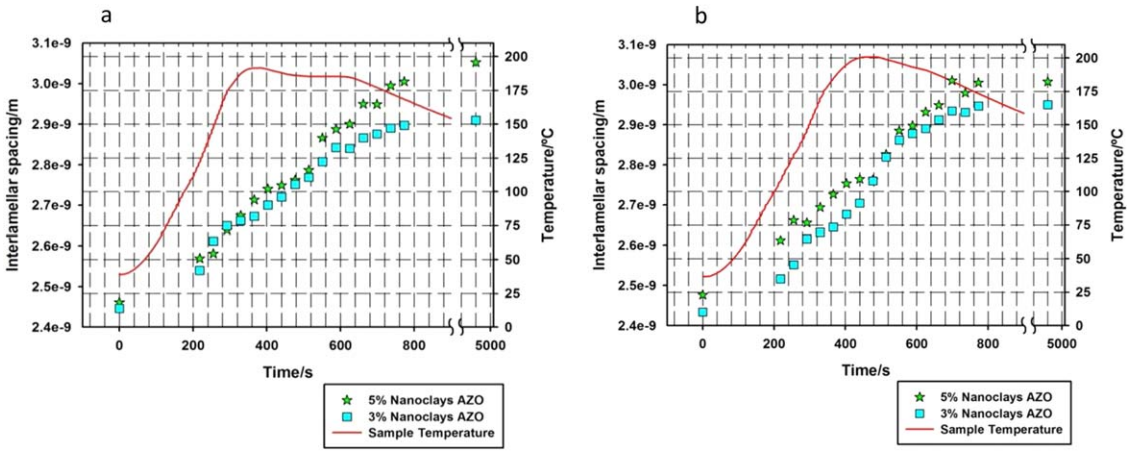

Figure 5. Evolution of the interlamellar spacing during foaming in samples containing different amounts of nanoparticles at foaming temperatures of (a) 185 and (b) 190 °C. [Color figure can be viewed in the online issue, which is available at wileyonlinelibrary.com.]

CONCLUSIONS

Synchrotron radiation has turned to be a very useful *in situ* technique for gaining new knowledge into the mechanisms involved in the increment of the intercalation degree of LDPE–clay nanocomposites during foaming with chemical blowing agents. The whole evolution of the interlamellar spacing during the foaming process was characterized for the first time.

Three blowing agents of very different natures were selected. Two of them released gas phases, one mainly nitrogen and the other one mainly carbon dioxide. In the case of the third blowing agent, the gas remained confined within the microspheres, and the swelling of these microspheres produced the expansion of the material. An increase in the interlamellar spacing during foaming took place to a higher or lower extent, independently of the blowing agent used. Therefore, a first important conclusion of this work was that the phenomenon was mainly associated with the foaming itself and not with the kind of gas or foaming procedure used.

The blending of nanoclays with AZO yielded higher exfoliation degrees during blending. On the contrary, blending with HY or EXP did not produce any effect on the exfoliation. These later samples presented a delamination state similar to the ones obtained when the blending was performed without any blowing agent. The initial exfoliation degree obtained with AZO also depended on the amount of AZO used. Higher additions yielded higher initial separations between platelets. Therefore, chemical interaction between AZO and organomodified nanoclays was postulated. This chemical interaction helped with the clay delamination during blending and was also connected with the catalytic effect of the used nanoclays in the decomposition temperature of AZO. It was proven that the gas was released at lower temperatures when the clay particles were included in the formulations and that a higher amount of gas was released when a higher amount of clay was added.

The increment in the interlamellar distance was not only promoted by foaming but also by the thermal mobility of the polymer molecular chains and the thermal expansion associated with the melting of the polymer. When the sample temperature increased, an increase in the interlamellar spacing was also observed. The movement of the polymer chains bonded to the edges of the nanoclays platelets separated them and contributed to their disorder. This effect was observed independently of the blowing agent nature, blowing agent addition, or nanoclay content, and it was basically associated with the nature of the polymeric matrix used and the degree of interaction between the clay platelets and the polymer.

There existed a correlation between the expansion ratio and the increment in interlamellar spacing. Higher increases in interlamellar distance were found in the samples with lower relative densities. For all of the samples, a maximum interlamellar spacing was reached during the foaming process. In the case of samples foamed with AZO, the maximum interlamellar spacing was maintained after foam collapse and solidification. On the contrary, in the samples foamed with the other two blowing agents, the interlamellar spacing found after collapse and solidification was lower than the maximum observed during the experiment. The postulated AZO–nanoclay interaction may have helped to keep the nanoclay platelets hooked to their new positions reached during foaming, even when the density of the materials increased because of a partial collapse of the cellular structure or the solidification of the polymeric matrix.

This scientific work has shown a new experimental methodology that allows one to follow *in situ* the exfoliation process of nanoclays. Foaming promoted the separation degree between platelets in the nanoclay-filled composite. As mentioned in the introduction, in noncomposite-containing clays, the highest possible exfoliation degree is sought. From this point of view, cellular materials benefit and present a higher intercalation degree than their initial solid matrices. The results shown in this article can be considered as an interesting synergetic effect between the use of nanoclays and foaming, because foaming promotes the intercalation of the nanoparticles.

ACKNOWLEDGMENTS

Financial assistance from the Ministerio de Economía y Competitividad and Federación Española de Enfermedades Raras (MAT 2012-34901), the Junta de Castile and Leon (VA035U13), and the European Spatial Agency (project MAP AO-99-075) is gratefully acknowledged. In addition, financial support through a Formación de Personal Investigador grant (BES-2013-062852 to B. Notario) and a Formación de Profesorado Universitario grant (AP2007-03319 to J. Escudero) from the Spanish Ministry of Education is gratefully acknowledged.

REFERENCES

1. Pavlidou, S.; Papaspyrides, C. D. *Prog. Polym. Sci.* **2008**, *33*, 1119.
2. Gilman, J. W. *Appl. Clay Sci.* **1999**, *15*, 31.
3. Utracki, L. A. Clay-Containing Polymeric Nanocomposites; Rapra Technology: Shawbury, United Kingdom, **2004**.
4. Golebiewski, J.; Rozanski, A.; Dzwonkowski, J.; Galeski, A. *Eur. Polym. J.* **2008**, *44*, 270.
5. Koo, J. H. Polymer Nanocomposites; McGraw-Hill: New York, **2006**.
6. Lee, E. C.; Mielewski, D. F.; Baird, R. *J. Polym. Eng. Sci.* **2004**, *44*, 1773.
7. Lam, C.; Lau, K.; Cheung, H.; Ling, H. *Mater. Lett.* **2005**, *59*, 1369.
8. Li, J.; Jiang, G. J.; Guo, S. Y.; Zhao, L. J. *Plast. Rubber Compos.* **2007**, *36*, 308.
9. Mainil, M.; Alexandre, M.; Monteverde, F.; Dubois, P. *J. Nanosci. Nanotechnol.* **2006**, *6*, 337.
10. Alexandre, M.; Dubois, P. *Mater. Sci. Eng.* **2000**, *28*, 1.
11. Gopakumar, T. G.; Lee, J. A.; Montopoulou, M.; Parent, J. S. *Polymer* **2002**, *43*, 5483.
12. Yasmin, A.; Abot, J. L.; Daniel, I. M. *Scr. Mater.* **2003**, *49*, 81.
13. Jin, Y. H.; Park, H. J.; Im, S. S.; Kwak, S. Y.; Kwak, S. *Macromol. Rapid Commun.* **2002**, *23*, 135.

14. Alexandre, M.; Dubois, P.; Sun, T.; Garces, J. M.; Jerome, R. *Polymer* **2002**, *43*, 2123.
15. Wang, S.; Hu, Y.; Zhongkai, Q.; Wang, Z.; Chen, Z.; Fan, W. *Mater. Lett.* **2003**, *57*, 2675.
16. Liang, G.; Xu, J.; Bao, S.; Xu, W. *J. Appl. Polym. Sci.* **2004**, *91*, 3974.
17. Ibeh, C. C.; Bubacz, M. *J. Cell. Plast.* **2008**, *44*, 493.
18. Zhai, W.; Park, C. B.; Kontopoulou, M. *Ind. Eng. Chem. Res.* **2011**, *50*, 7282.
19. Zeng, C.; Han, X.; Lee, L. J.; Koelling, K. W.; Tomasko, D. L. *Adv. Mater.* **2003**, *15*, 1743.
20. Lee, Y. H.; Wang, K. H.; Park, C. B.; Sain, M. *J. Appl. Polym. Sci.* **2007**, *103*, 2129.
21. Seraji, S. M.; Aghjeh, M. K. R.; Davari, M.; Hosseini, M. S.; Khelgati, S. *Polym. Compos.* **2011**, *32*, 1095.
22. Saha, M. C.; Kabir, M. E.; Jeelani, S. *Mater. Sci. Eng. A* **2008**, *479*, 213.
23. Gorem, K.; Chen, L.; Schadler, L. S.; Ozisik, R. *J. Supercrit. Fluids* **2010**, *51*, 420.
24. Verdejo, R.; Saiz-Arroyo, C.; Carretero-Gonzalez, J.; Barroso-Bujans, F.; Rodriguez-Perez, M. A.; Lopez-Manchado, M. A. *Eur. Polym. J.* **2008**, *44*, 2790.
25. Bernal, M. M.; Molenberg, I.; Estravis, S.; Rodriguez-Perez, M. A.; Huynen, I.; Lopez-Manchado, M. A.; Verdejo, R. *J. Mater. Sci.* **2012**, *47*, 5673.
26. Saiz-Arroyo, C.; Escudero, J.; Rodriguez-Perez, M. A.; De Saja, J. A. *Cell. Polym.* **2011**, *30*, 63.
27. Saiz-Arroyo, C.; Rodriguez-Perez, M. A.; Velasco, J. I.; Saja, J. A. D. *Compos. B* **2013**, *48*, 40.
28. Velasco, J. I.; Antunes, M.; Ayyad, O.; Saiz-Arroyo, C.; Rodríguez-Pérez, M. A.; Hidalgo, F.; de Saja, J. A. *J. Appl. Polym. Sci.* **2007**, *105*, 1658.
29. Velasco, J. I.; Antunes, M.; Ayyad, O.; López-Cuesta, J. M.; Gaudon, P.; Saiz-Arroyo, C.; Rodríguez-Pérez, M. A.; de Saja, J. A. *Polymer* **2007**, *48*, 2098.
30. Reyes-Labarta, J. A.; Marcilla, A. *J. Appl. Polym. Sci.* **2008**, *107*, 339.
31. Bhatti, A. S.; Dollimore, D.; Goddard, R. J.; O'Donnell, G. *Thermochim. Acta* **1984**, *76*, 63.
32. Gomes, M. E.; Godinho, J. S.; Tchalamov, D.; Cunha, A. M.; Reis, R. L. *J. Appl. Med. Polym.* **2002**, *6*, 75.
33. Qin, X.; Thompson, M. R.; Hrymak, A. N. *Polym. Eng. Sci.* **2007**, *47*, 522.
34. Bledzki, A. K.; Faruk, O. *J. Cell. Plast.* **2005**, *41*, 539.
35. Andersson, H.; Griss, P.; Stemme, G. *Sens. Actuators B* **2002**, *84*, 290.
36. Yao, J.; Barzegari, M. R.; Rodrigue, D. *Cell. Polym.* **2010**, *20*, 5.
37. Solorzano, E.; Laguna, E.; Perez, S.; Kaestner, A.; Rodriguez-Perez, M. A. *Colloids Surf. A* **2015**, *473*, 46.